Final Draft
of the original manuscript:

Ferri, O.M.; Ebel, T.; Bormann, R.:
Influence of Surface Quality and Porosity on Fatigue Behaviour of Ti-6Al-4 V Components Processed by MIM
In: Materials Science and Engineering A (2009) Elsevier

DOI: 10.1016/j.msea.2009.11.007

Influence of Surface Quality and Porosity on Fatigue Behaviour of Ti-6Al-4V Components Processed by MIM

Authors: O.M. Ferri, T. Ebel, R. Bormann

Affiliation: GKSS Research Center, Institute of Materials Research, Max-Planck-Str. 1, D-21502 Geesthacht, Germany

Abstract

Fatigue and tensile mechanical properties of Ti-6Al-4V alloy processed by metal injection moulding (MIM) technology were evaluated in this investigation. Two critical parameters, binder content of the feedstock and maximum sintering temperature, were studied. Samples sintered at 1350 °C exhibited higher tensile strength than those sintered at 1250 °C. Higher content of binder promoted an increase of the surface quality of MIM components. Consequently, the fatigue endurance limit increased from ~350 MPa (components with lower binder content) to ~400 MPa (samples with a higher binder content). Furthermore, reduction of ductility was observed for changing from closed to open porosity; however, the fatigue resistance did not follow the same trend. This is probably due to the fact that better surface quality and smaller grain size compensated the negative influence of porosity on the fatigue behaviour.

Keywords: MIM; Four-point bending fatigue; Ti-6Al-4V alloy; Binder content; Sintering temperature.

1. Introduction

Research of titanium and its alloys is of great interest because of the unique combination of high specific strength and excellent corrosion resistance [1]. However, due to the rather high costs of processing and raw material, the use of these alloys in mass production remains limited. One possible process candidate that can potentially provide a reduction of the manufacturing costs is the metal injection moulding (MIM) technique. MIM processing offers many unique advantages for the mass production of near neat-shape components. It combines the shaping efficiency of plastic injection moulding with the capability of powder metallurgy [2]. Today, it is possible to fabricate Ti-6Al-4V alloy by MIM technology with tensile properties in the range of wrought material [3]. Nevertheless, there is still reluctance to use the MIM process to fabricate components that will be exposed to fatigue. The concern is related to the fatigue property degradation due to the presence of residual porosity. Recent investigations [4-6] of the effect of MIM processing on the fatigue strength of Ti-6Al-4V alloy showed that the fatigue strength is in the range of 350 to 380 MPa at 10^7 cycles compared to around 600 MPa for wrought material. These results demonstrate that it is necessary to further increase the fatigue resistance of components fabricated by MIM in order to reach the performance levels of the wrought Ti-6Al-4V alloy. Shot peening sintered MIM samples promoted a remarkable increase of approximately 100 MPa on the fatigue endurance limit. Possible reasons that can explain such an increase are related to local plastic deformation and internal stress generation due to the shot peening [5] and also to a partial closing of surface pores. Further efforts [6] were

carried out in order to optimize the fatigue behaviour of MIM components by using an initial powder diameter of below 25 µm instead of 45 µm for standard MIM process. However, only a marginal increase of 30 MPa was observed in MIM samples with finer particle size. Altogether, the studies showed the well-known importance of surface quality for high fatigue resistance. A further critical parameter with regard to surface quality is the rheological behaviour of the feedstock during mould filling, which is related to among others things, to the binder content. Therefore, in this study, specimens with different binder content and different maximum sintering temperatures were fabricated by the MIM technique. Four point bending fatigue tests, tensile tests, microstructure and fracture surface analyses were carried out in order to describe the influence of these parameters on the fatigue behaviour of Ti-6Al-4V alloy processed by MIM.

2. Experimental

Spherical gas-atomised Ti-6Al-4V alloy powder fabricated by TLS Technik GmbH, Germany, was used in this investigation. The powder diameter was below 45 µm. The impurity levels of the powder were: 880 µg/g in O, 165 µg/g in N and 20 µg/g in C. The feedstock, a mixture of the metallic powder and a polymer binder system, was prepared under argon atmosphere in a Z-blade mixer at a temperature of 120°C for 2 hours. The binder system used in this study consisted of 60 wt.% paraffin wax, 35 wt.% polyethylene vinyl acetate (EVA) and 5 wt.% stearic acid. In order to evaluate the influence of the binder content on the fatigue performance of Ti-6Al-4V alloy, two binder system fractions, 31 vol.

% and 35 vol. %, were used for feedstock preparation. A more detailed description of the MIM process performed can be found in [7].

An Arburg 320S machine was used for the injection moulding of the feedstock. Two different geometries were produced: a bending fatigue specimen (Fig. 1) and a standard "dog-bone" tensile test specimen (Fig. 2). After injection of the components, the binder was removed from the specimen by chemical and thermal debinding processes. The chemical debinding was applied in order to remove the paraffin wax fraction of the binder system. The samples were immersed in heptane at 40 °C for 20 hours. The thermal debinding of the remaining binder and the sintering were conducted in a single-step heat treatment run.

Differences in the binder content of the feedstock produced different particle distances prior to sintering. Therefore, in order to have approximately the same level of porosity after sintering without prolongation of the process time, the samples were sintered at different maximum temperatures. Two maximum sintering temperatures (1250 °C and 1350 °C) were used in this study. The holding time at maximum temperature was 2 hours in both cases.

The relative densities of green (after injection) and sintered samples were determined by the immersion method (Archimedes's principle) outlined in ASTM B311. Conventional LECO melt extraction systems were used to determine the impurity levels of oxygen, nitrogen and carbon. Surface roughness was estimated by using a Hommel tester T1000.

High-cycle four point bending fatigue tests were performed on a resonance machine fabricated by RUMUL. The experiments were carried out under load control with a cyclic frequency of ~95 Hz (sine wave) at a load ratio $R=\sigma_{min}/\sigma_{max}$ of 0.2. A fatigue endurance limit or "runout" for the tests was defined as 10^7 cycles. All the experiments were conducted in air at room temperature. Two complete S-N curves were made, one referring to samples with a binder system fraction of 31 vol. % sintered at 1250 °C and the other one referring to samples with a binder system fraction of 35 vol. % sintered at 1350 °C. Additionaly, nine samples with binder content of 35 vol. % sintered at 1250 °C were tested at three different stress levels. This last experiment was carried out in order to evaluate the influence of maximum sinter temperature on the fatigue behaviour. In the following the samples fabricated with a binder system fraction of 31 vol. % sintered at 1250 °C will be referred as MIM31L and the samples with a binder system fraction of 35 vol. % sintered at 1250 °C and 1350 °C will be referred as MIM35L and MIM35H, respectively.

Tensile tests were performed on a servohydraulic structural test machine equipped with a 100 kN load cell. The tensile tests were carried out at room temperature at a strain rate of 1.2×10^{-5} s^{-1}. Light microscopy was used to investigate the microstructure. The fracture surface of tensile and fatigue specimens were analysed by a scanning electron microscope (ZEISS – DSM962). The alpha colony size and the pore size were estimated by using an image analysis system.

3. Results and discussion

3.1. Microstructural features and chemical composition

Table 1 shows the microstructural features and chemical composition of Ti-6Al-4V samples. With increasing binder content the green density decreased as expected. The bulk density of the Ti-6Al-4V alloy component without pores was determined to be 4.41 g/cm^3 after measuring a sample exposed to an additional HIP process following the MIM production. Therefore, it was possible to estimate the porosity of the sintered samples by using:

$$Porosity\ [\%] = 100 - \left[\left(\frac{\rho_0}{\rho_B}\right) \bullet 100\right] \quad (1)$$

Where ρ_0 is the apparent sintered or the apparent green density measured by immersion method and ρ_B is the apparent bulk density of Ti-6Al-4V alloy component without pores.

As noted in Table 1, the MIM35L samples present the highest porosity value (approximately 6 %). Moreover, it is important to note that the MIM35H samples and the MIM31L samples show approximately the same amount of porosity (approximately 3.5 %). This means the larger initial particle distance was compensated for by applying a higher sintering temperature.

No significant difference in the level of impurities was observed amongst the three different configurations. This is related to a relatively constant furnace atmosphere during sintering

over different heating cycles. The variation of the oxygen content is even in the common range for this material: between 2000 µg/g and 2300 µg/g.

The increase of sintering temperature promoted an increase in α colony size due to the tendency of coarsening mechanism over densification mechanisms during sintering process at higher temperatures. In addition, contrary to the MIM31L and MIM35L samples, a well defined continuous α layer at β grain boundaries is observed in the MIM35H samples (Fig. 3). However, the size of the continuous α layer is not crucial with respect of the ductility of this alloy since no significant strength difference between the α colony lamellae and the continuous α layers is expected [8]. The α colonies are not well defined in the MIM35L samples (Fig. 4). This is a result of insufficient temperature and time for the development of the microstructure during the sintering process. Additionally, the irregular shape of the pores together with some pore cluster regions are further indication of an inadequate sintering process, probably leading to the presence of interconnected porosity instead of closed porosity. One can assume that the MIM31L samples (Fig. 5) and the MIM35H samples (Fig. 3) exhibit a closed porosity since the pores are isolated and rounded. Additionally, the amount of porosity derived from the relative density is below 5 % (see Table 1), which is commonly accepted limit between open and closed porosity [10]. Fig. 6 exhibits a typical pore diameter distribution for the MIM35L samples. The maximum pore diameter observed and the P_{90} (90% of the analysed pores exhibited a diameter below the P_{90} value) are summarised in Table 2 for the MIM31L, MIM35L and MIM35H samples.

3.2. Tensile properties and tensile fractography

The tensile properties of the three studied configurations are summarized in Table 3. Under monotonic tensile loading, porosity reduces the effective cross-sectional area for load bearing and acts as a stress concentration site for strain localization and damage, leading to strength and ductility reduction [9]. This trend was also observed in this investigation. However, it is important to note that the elongation values obtained for MIM31L samples and MIM35H samples are still higher than the minimal values required in the ASTM B 348-2 for this respective alloy under wrought condition. This behaviour is not unexpected since macroscopic ductility is not severely affected by the presence of isolated porosity [10]. On the other hand, the presence of interconnected porosity is more detrimental and reduces macroscopic ductility to a greater extent. Therefore, the presence of interconnected porosity in the MIM35L samples (as mentioned in the previous section) can explain the smaller elongation rather than the difference in strength, when compared MIM35L with MIM35H samples.

Usually the increase of grain size promotes a degradation of the mechanical properties. However, in our study the increase of α colony size observed in the MIM35H samples did not result in a decrease of strength or ductility. As the MIM31L samples and MIM35H samples have nearly the same apparent density and impurity levels, the higher tensile strength of the MIM35H samples has to be associated with some other effect involved by the higher sintering temperature. This effect overcomes the influence of grain size on mechanical properties as supported by the higher amount of “fine dimples”(indicated by

white arrow) on the fracture surface of MIM35H samples (Fig. 7) compared to MIM31L samples (Fig. 8). Furthermore, the formation of "fine dimples" was less pronounced in the fracture surface of the MIM35L samples (Fig. 9), which was also sintered at lower temperature. However, the exact mechanism behind the formation of the fine dimples on the fracture surface of the samples sintered at higher temperature can not be explained in the present investigation. Therefore, future work is planned in order to study this phenomenon.

The presence of these dimples on the tensile fracture surface of Ti-6Al-4V alloy without pores has been reported on the literature before [11, 12]. The dimensions of the dimples shown in these investigations are in the same range as those observed in this study for MIM35H samples, here referred to "fine dimples". In contrast, for Ti-6Al-4V alloy produced by MIM, Zhang et al.[3] proposed as the typical ductile dimple structure a surface similar to the fracture surfaces of the MIM31L and MIM35L samples, here referred to as "coarse dimples". Such a coarse structure is also present in the fracture surface of MIM35H samples (region inside the white ellipse in Fig. 7); however, its occurrence is less pronounced than in the case of MIM31L and MIM35L samples, due to the presence of areas with fine dimples. Therefore, as mentioned before, the maximum sintering temperature seems to be a critical factor for increasing the "fine dimples" structure in the tensile fracture surface.

3.3. Fatigue behaviour

The four point bending fatigue behaviour of MIM samples with different binder content and different maximum sintering temperatures is shown in Fig. 10. The MIM35H samples demonstrate a superior endurance limit (~400 MPa) when compared with MIM31L samples (~350 MPa). Several authors [13-17] assumed that the fatigue resistance of powder metallurgy materials is mainly controlled by porosity. However in terms of porosity, it is not possible to explain the fatigue behaviour difference of MIM31L and MIM35H samples since the amount of porosity is almost identical for the two configurations. Furthermore, the grain size difference between the two configurations cannot explain for the fatigue behaviour difference either since the relatively coarser microstructure exhibits the higher fatigue resistance. Therefore, other mechanisms have to cause such behaviour. One possible explanation is the fact that fatigue behaviour is very sensitive to surface quality, especially under bending conditions. As it can be seen in Fig. 11(MIM31L) and Fig. 12 (MIM35H) the surface quality appears to be different in terms of surface roughness. It is interesting to note that however the roughness measurement revealed no significant difference on the R_a values for MIM31L (R_a=1.95 μm) and MIM35H (R_a=2.08 μm), due to the fact that the tip of the Hommel tester T1000 equipment is not able to measure irregular surface defects such as those presented in Fig. 11.

As reported in [5], the notches observed are located directly on the surface and they are most likely created during the injection or during the debinding process. Therefore, we conclude that a higher content of binder promotes a better surface quality for the injected

samples. The explanation for such behaviour is most likely related to the lower viscosity of the feedstock when a higher binder content is used. As a consequence, during injection, the powder particles in the feedstock with the higher amount of binder are able to fill a possible surface defect more easily. This is mainly due to lower friction between the particles and the mould walls. In addition, the shear forces between the particles and the mould wall are reduced, improving the filling behaviour. On the other hand, it is important to point out that a higher binder content of the feedstock requires a higher sintering temperature or a longer sintering time in order to achieve the same densification of a component with lower binder content. Consequently, it is necessary to find a compromise between surface quality (binder content) and the sintering process (cost and time).

Fractography of fatigued specimens revealed the possible region for the crack nucleation of MIM31L (Fig. 14) and MIM35H (Fig. 15). The maximum observed size of the notches located at the surface of the samples was approximately 100 µm and 50 µm for MIM31L and MIM35H, respectively. Notches are well known to exhibit a negative influence on the fatigue properties [18, 19], thus, the differing results in fatigue resistance of MIM31L and MIM35H can be related to surface roughness differences.

Another possible explanation for the higher fatigue strength of MIM35H compared to MIM31L is the influence of the sintering parameters on the mechanical properties. As described in the previous section, the increase of maximum sintering temperature results in an improvement of the tensile properties together with an apparently higher presence of fine dimples on the tensile fracture surface. Results presented by Hadrboletz and Weiss [9]

for Fe-2C-2.5Ni samples made by powder metallurgy showed that fatigue strength increases when a more intensive sintering process (higher temperature, longer sintering time) has been chosen.

Surprisingly, the MIM35L samples apparently achieved fatigue behaviour similar to that of the MIM35H samples (Fig. 10). This result is unexpected since the MIM35L presented higher porosity (5.7 % compared to 3.6 % of MIM35H) and poorer tensile properties. However, it is possible to explain this behaviour with Fig. 4, which illustrates that the MIM35L samples exhibit a finer microstructure when compared to MIM35H (Fig. 3). It is well known that a refinement of the microstructure leads to an increase of the high cycle fatigue resistance [20, 21]. In fact, refinement of the microstructure means reduction of the slip length and, consequently, reduction of the number of dislocation pile-ups at critical preferential locations (pores and grain boundaries) for crack nucleation. Therefore, it is reasonable to assume that a refinement of the microstructure (smaller slip length) can compensate for the negative influence of the porosity on the fatigue behaviour of components fabricated by MIM technology.

Furthermore, Fig. 10 shows that the MIM35L samples exhibit a better fatigue behaviour than MIM31L. This behaviour is expected since as illustrated in Fig. 11 and Fig 13, the MIM35L samples present smaller surface defects than MIM31L samples. Obviously, the refinement of the microstructure (grain size), together with a better surface quality compensate for the negative influence of porosity with respect to high cycle fatigue behaviour. Although pores with a diameter of approximately 90 µm were observed in the

interior of the MIM35L samples, the maximum observed size of the notches located at the surface was only approximately 50 μm (Fig. 16). Nevertheless as indicated in Table 3, for the tensile mechanical properties, the refinement of the microstructure (smaller grain size) and a better surface quality apparently are secondary effects while the amount, size and distribution of the porosity are the determinant parameters.

4. Conclusions

The effects of binder content of the feedstock and the maximum sintering temperature on the quasi-static and fatigue properties of Ti-6Al-4V alloy produced by metal injection moulding were investigated. The increase of maximum sintering temperature led to an increase of tensile strength. Although a higher binder content and higher sintering temperature were tested, no significant difference in impurity levels was observed amongst the different configurations. A better surface quality was achieved by using a feedstock with a higher binder content. The reason for such behaviour is probably related to differences in the mould filling behaviour due to changing the feedstock viscosity. Furthermore, the better surface quality (lower defect size on the surface) is the main reason for the superior fatigue behaviour of samples processed with a higher content of binder than those with lower content of binder. A clear relationship between the type of porosity (open or closed) and the tensile properties was observed. However, the variation of the porosity (3.6 % to 5.7 %) surprisingly did not affect the fatigue behaviour of Ti-6Al-4V alloy components fabricated by MIM. This is an indication that, at these specific porosity levels,

the grain size and size of surface defects (surface quality) are the main factors that influence the fatigue behaviour of Ti-6Al-4V alloy processed by MIM, not the porosity.

References

[1] S. Ankem, C. A. Greene, Mater. Sci. Eng. A 236 (1999) 127-131.

[2] R. M. German, Powder Injection Molding, MPIF, New York, 1990.

[3] R. Zhang, J. Kruszewski, J. Lo, Powder injection moulding international 2 (2008) 74-78.

[4] M. Niinomi, T. Akahori, M. Nakai, K. Ohnaka, Innovations in Titanium Technology, in: M. N. Gungor, M. A. Imam, F. H. Froes (Eds.), TMS2007 136th Annual meeting & exhibition, 2007, pp. 209-217.

[5] O.M. Ferri, T. Ebel, R. Bormann, Mater. Sci. Eng. A 504 (2009) 107-113.

[6] O.M. Ferri, T. Ebel, R. Bormann, Fatigue property of Ti-6Al-4V components fabricated by metal injection moulding, in: EURO PM2008, Manheim, 2008.

[7] W. Limberg, E. Aust, T. Ebel, R. Gerling, B. Oger, Metal injection moulding of an advanced bone screw 7Nb alloy powder, in: H. Danninger, R. Ratzi (Eds.), EURO PM 2004, vol 4, 2004.

[8] G. Lütjering, Mat. Scie. and Eng. A 243 (1998) 32-45.

[9] A. Hadrboletz, B. Weiss, Inter. mat. review 42 (1997) 1-44.

[10] B. Weiss, R. Stickler, H. Sychra, Met. Powder Rep. 45 (1990) 187-192.

[11] B. Venkatesh, D.L. Chen, S. D. Bhole, Scripta Materialia 59 (2008) 291-394.

[12] E. D. Tabachnikova, A. V. Podolskiy, V. Z. Bengus, S. N. Smirnov, M. I. Bidylo, K. Csach, J. Miskuf, L. R. Saitova, I. P. Semenova, R. Z. Valiev, Mat. Scie. and Eng. A (2008).

[13] N. Chawla, T.F. Murphy, K.S. Narasimhan, M. Koopman, K. K. Chawla, Mat. Scie. and Eng. A380 (2001) 180-188.

[14] N. Chawla, X. Deng, Mat. Scie. and Eng. A390 (2005) 98-112.

[15] R. B. Wassenberg, O. F. Nurol, P. Beiss, Bending fatigue of a high performance PM steel, in: Europm 2004, vol 3, 2004.

[16] C. Xu, B. Weiss, G. Khatibi, H. Danninger, Ultra high cycle fatigue behaviour of high density PM alloy steels, in: EUROPM 2004, 2004.

[17] S. S. S. Akaslan, R. J. Causton, W. B. James, T. F. Murphy, A. Lawley, Effect of porosity and microstructural inhomogeneities on the fatigue crack growth response of a sinter-hardenable hybrid PM steel, in: Euro PM2004, vol 3, 2004, pp. 117-126.

[18] D. B. Lanning, T. Nicholas, G. K. Haritos, Inter. J. Fatigue 27 (2005) 45-57.

[19] G. K. Haritos, T. Nicholas, D. B. Lanning, Inter. J. Fatigue 21 (1999) 643-652.

[20] C. A. Stubbington, A. W. Bowen, J. Mat. Sci. 9 (1974) 941-947.

[21] J. Mueller, T. Ludian, H.J. Rack, L. Wagner, Microstructural and mean stress effects in fatigue performance of shot peened Ti-6Al-4V, in: M. Ninomi, S. Akiyama, M. Ikeda, M. Hagiwara, K. Maruyama (Eds.), Ti-2007 science and technology, 2007, pp. 375-378.

Figures

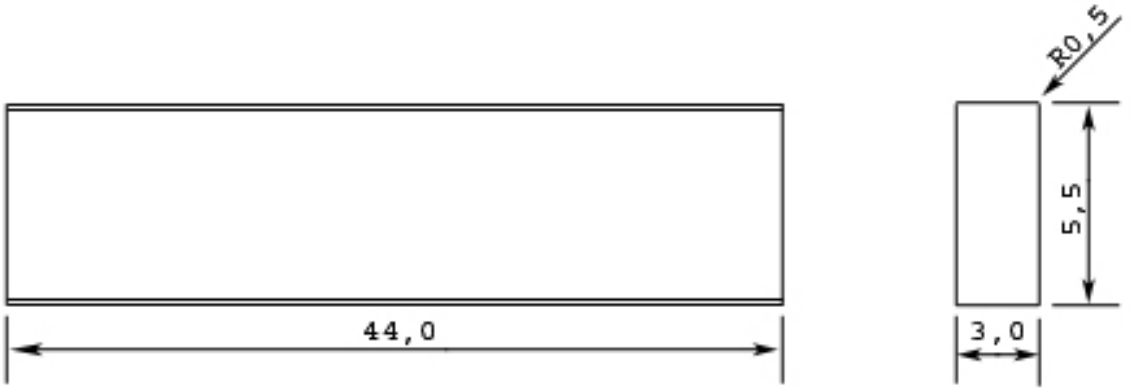

Fig. 1. Geometry of bending fatigue specimens. Dimensions of samples as sintered condition. Units are in millimetres.

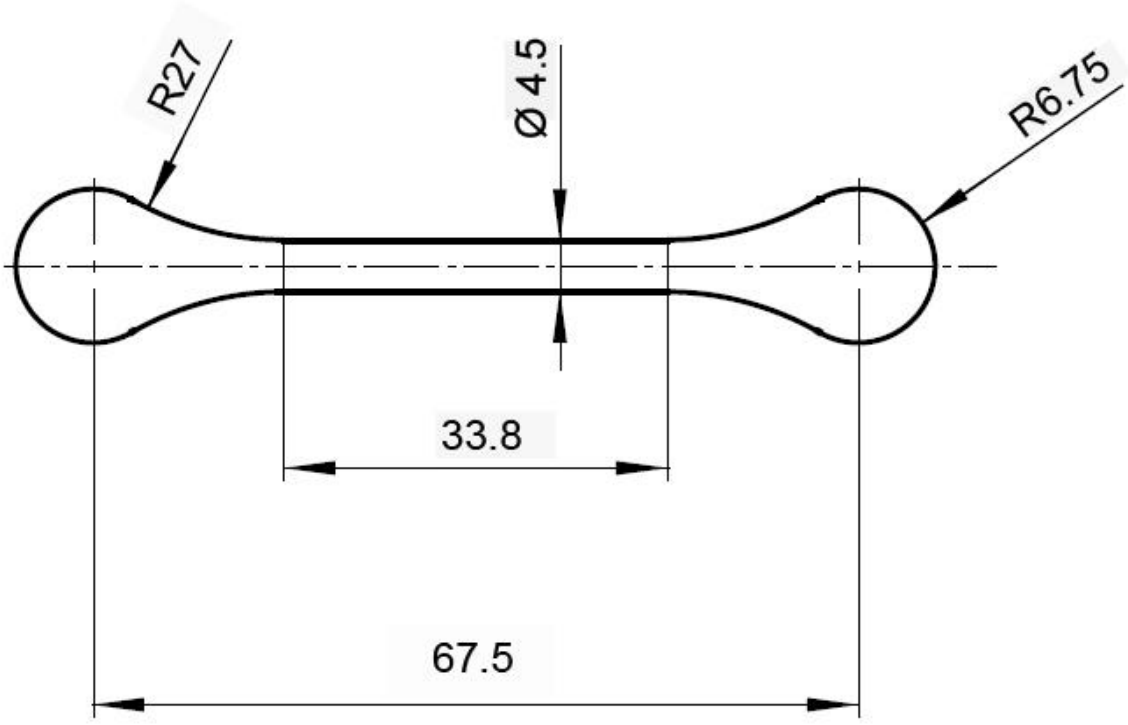

Fig. 2. Geometry of "dog-bone" tensile test specimen. Dimensions samples as sintered condition. Units are in millimetres.

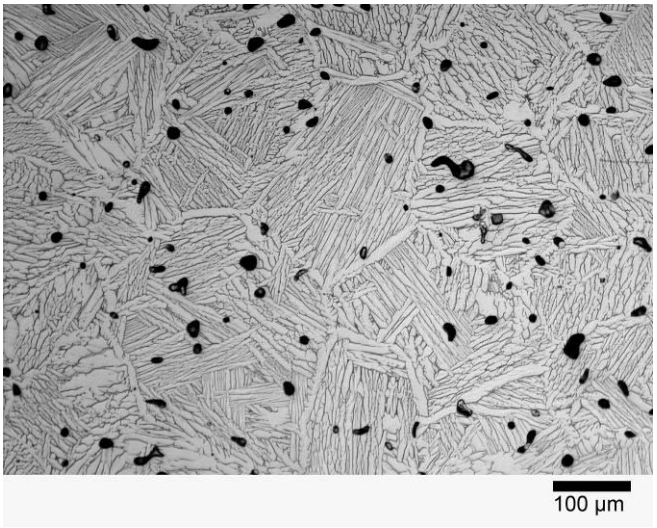

Fig. 3. Microstructure of MIM35H samples. Pores are correlated with the black regions.

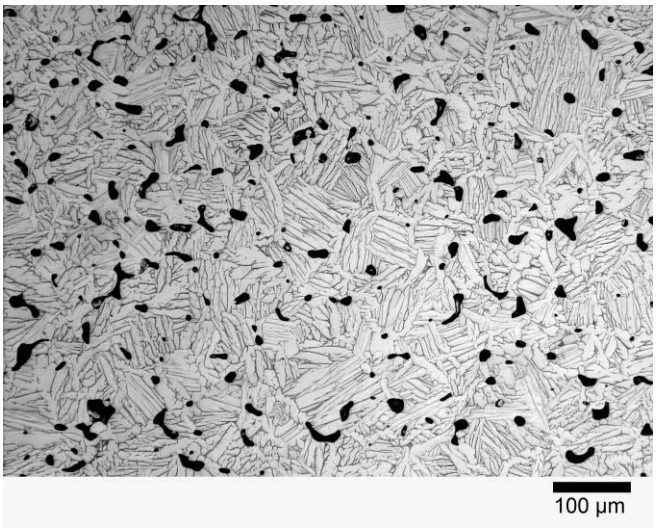

Fig. 4. Microstructure of MIM35L samples. Pores are correlated with the black regions.

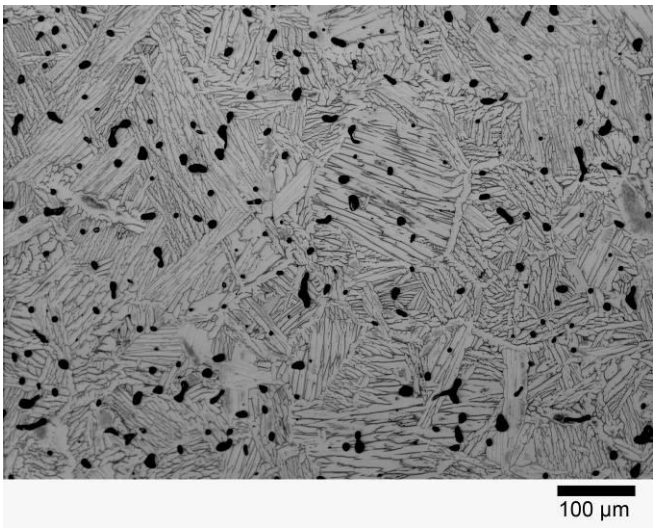

Fig. 5. Microstructure of MIM31L samples. Pores are correlated with the black regions.

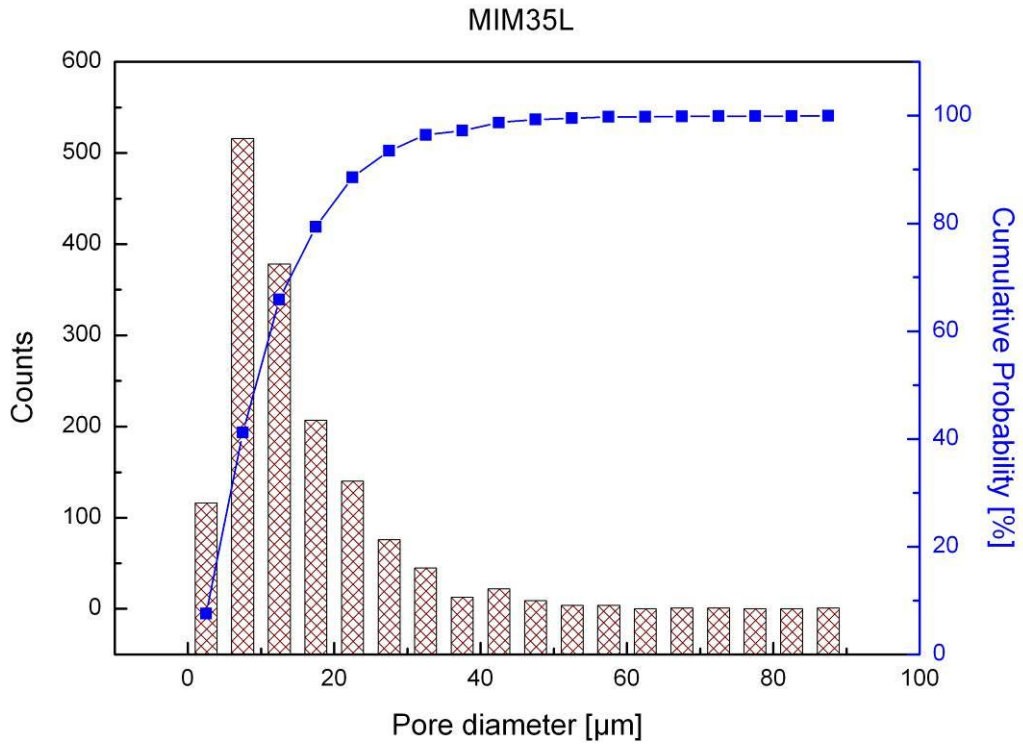

Fig. 6. Pore diameter distribution and cumulative probability for MIM35L samples.

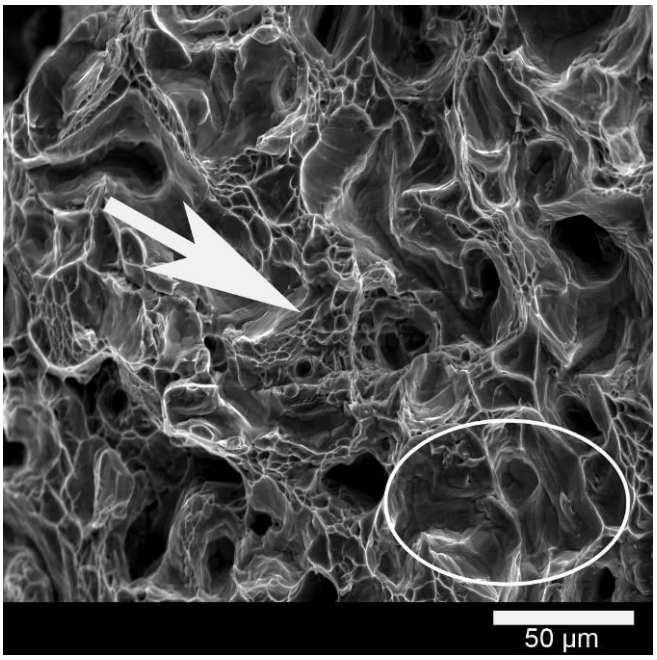

Fig. 7. Tensile fracture surface of MIM35H samples. Pores and dimples are visible.

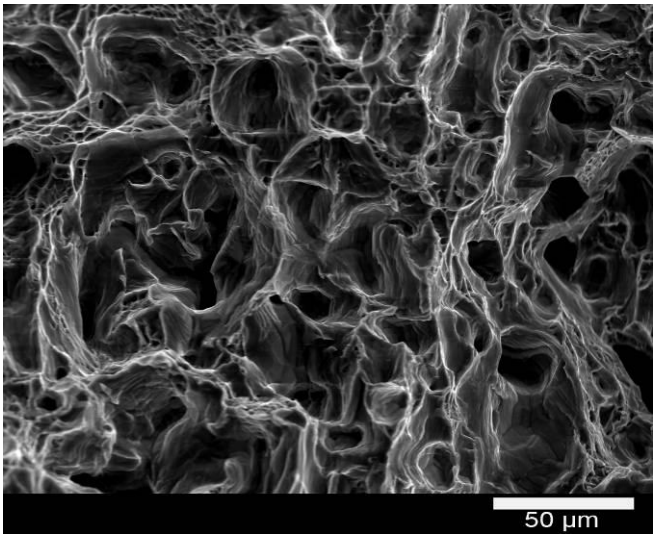

Fig. 8. Tensile fracture surface of MIM31L samples. Pores and dimples are visible.

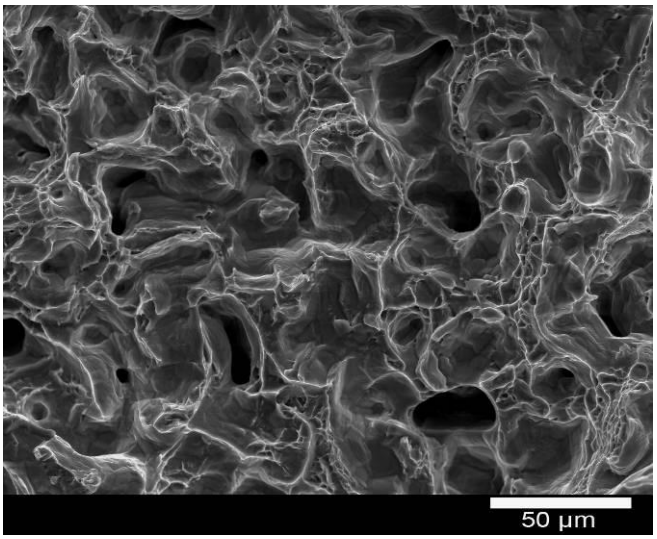

Fig. 9. Tensile fracture surface of MIM35L samples. Pores and dimples are visible.

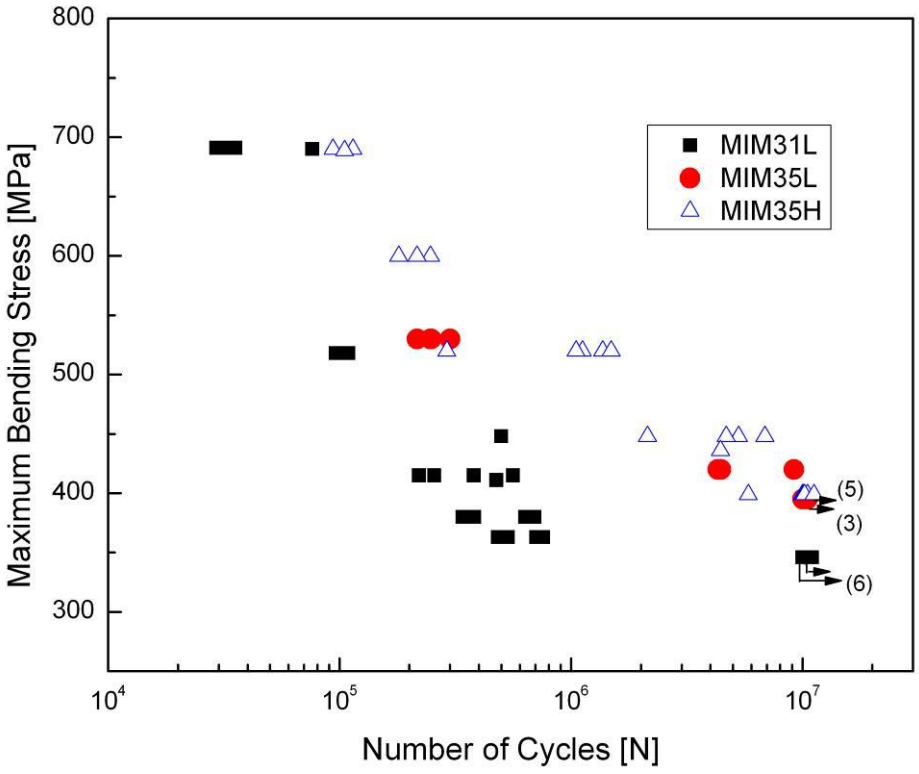

Fig. 10. S-N curves for MIM31L, MIM35L and MIM35H samples.

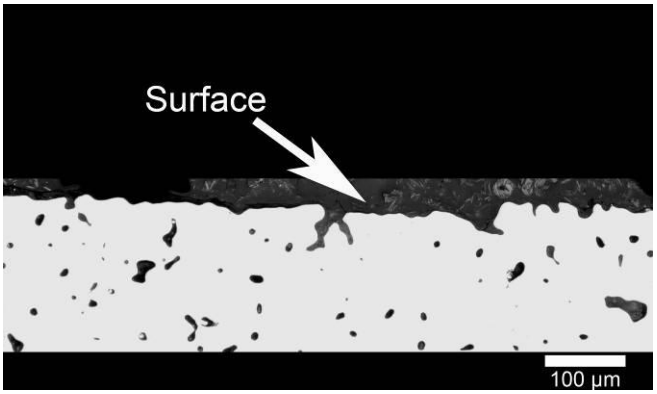

Fig. 11. Surface quality of MIM31L samples.

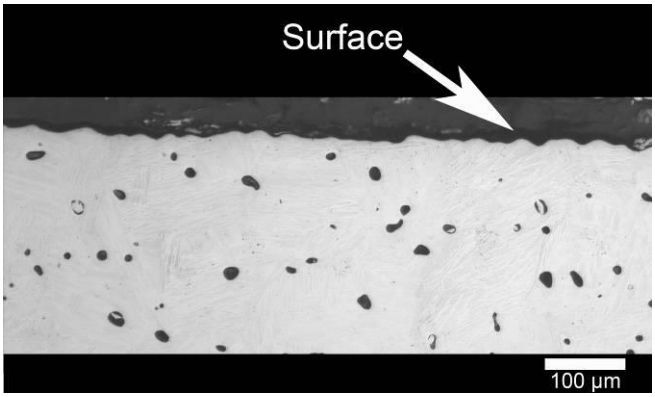

Fig. 12. Surface quality of MIM35H samples

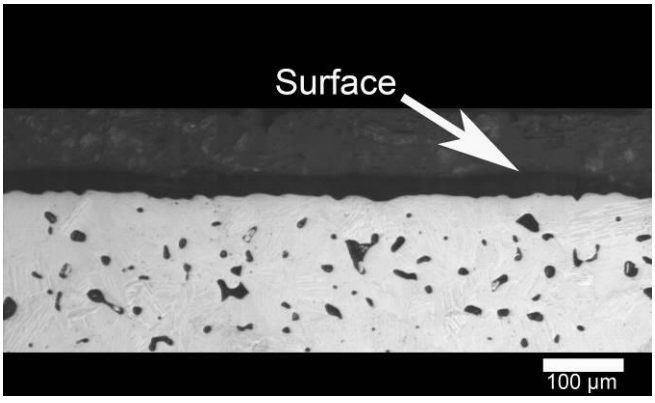

Fig. 13. Surface quality of MIM35L samples.

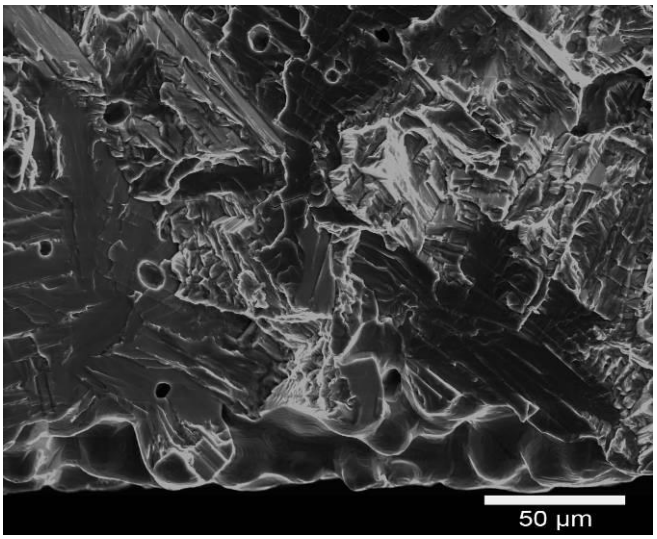

Fig. 14. Typical fracture surface of MIM31L samples.

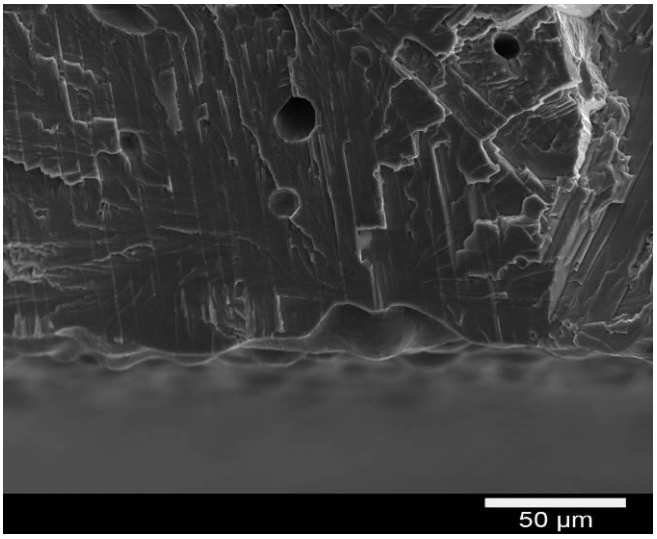

Fig. 15. Typical fracture surface of MIM35H samples.

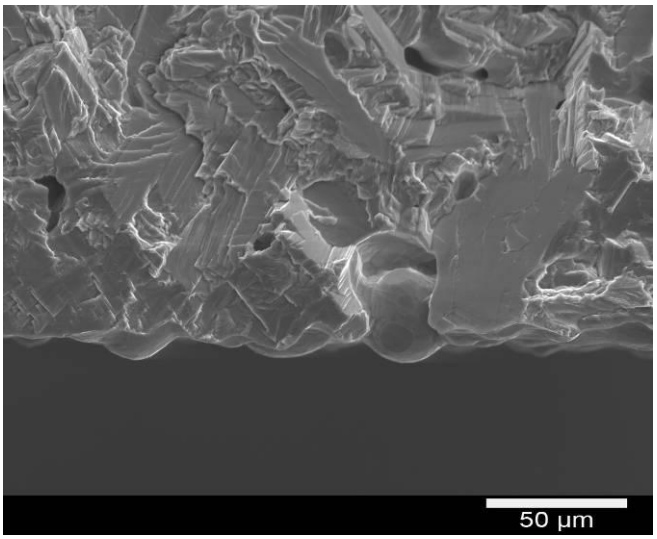

Fig. 16. Typical fracture surface of MIM35L samples.

Tables

Microstructure Features	MIM31L	MIM35H	MIM35L
Green density [g/cm^3]	3.31	3.2	3.2
Sinter density [g/cm^3]	4.26	4.25	4.16
Porosity [%]	3.4	3.6	5.7
α colony size [µm]	97	148	93
Average C content [µg/g]	370	409	422
Average N content [µg/g]	222	172	190
Average O content [µg/g]	2128	2318	2066

Table 1. Microstructural features of samples sintered at a maximum temperature of 1250 and 1350 °C with different binder content.

Porosity distribution	MIM31L	MIM35H	MIM35L
Max. pore diameter [µm]	33	47	87
P_{90} [µm]	17	20	24

Table 2. Maximum pore diameter and the P_{90} value (see text).

Tensile property	MIM31L	MIM35H	MIM35L
Yield Stress [MPa]	703 ± 3	720 ± 2	680 ± 2
Maximum Stress [MPa]	806 ± 3	824 ± 4	784 ± 0.8
Elongation [%]	13.7 ± 1	13.4 ± 0.7	10.8 ± 0.3
Fracture Surface [-]	Almost no fine dimples	More fine dimples	Almost no fine dimples

Table 3. Tensile property and fracture surface analysis.